

## Effect of surface nanocrystallization on corrosion behaviour of coated steel in chloride solution

Liuyan Zhang<sup>\*</sup>, Shuimei Yang, Huishu Wu, Xiaohua Jie<sup>\*</sup>, Xiaoye Huang, Xiujin Wang

School of Materials and Energy, Guangdong University of Technology, Guangzhou 510006, PR China

<sup>\*</sup>E-mail: [zlyjust@gdut.edu.cn](mailto:zlyjust@gdut.edu.cn)

Received: 20 November 2017 / Accepted: 18 January 2018 / Published: 6 March 2018

---

A nanocrystalline (NC) layer was fabricated on the surface of the low-alloy steel 15CrMo using high-energy shot peening. Two kinds of conversion coatings including the chemical conversion coating and electrochemical conversion coating were separately prepared on the surface of the original coarse-grained (CG) and the NC steel. The morphology and corrosion behavior of the different conversion coatings on the CG and NC surface were evaluated. The results indicated that after surface nanocrystallization of 15CrMo steel, the main changes due to the chemical conversion coating on its surface were the amorphization of the regular crystallized particles and more alloy elements in the film. The film formation characteristics of the electrochemical conversion coating did not change as much. The chemical conversion coating on the NC steel had higher corrosion resistance than that on the CG steel due in large part to the self-passivation elements joining in the film and the dense structure of the film. However, the electrochemical conversion coating on the NC steel had higher corrosion resistance than that on the CG steel due to its stronger adhesion to substrate. Surface nanocrystallization of the steel substrate can effectively improve the corrosion resistance of the conversion coating.

---

**Keywords:** nanocrystalline; steel; conversion coating; morphology; corrosion resistance

### 1. INTRODUCTION

Nanocrystalline (NC) materials have gained interest due to their unique mechanical and chemical properties[1,2]. High-energy shot peening is an effective severe plastic deformation method to fabricate a NC layer on metals. This is known as surface nanocrystallization[3-5]. Compared to the extensive attention given to the mechanical properties of the surface NC metals [6-8], research on their corrosion behavior—especially anti-corrosion methods—is much more rare. Ralston et al. explained how the grain size affects the corrosion rate and passivation of various metals[9,10]. Liu et al. found that the corrosion rate would increase after nanocrystallization of the metals if the corrosion products

were dissoluble; however, the corrosion rate would decrease if the corrosion products were insoluble, [11].

Low-alloy steel has better mechanical properties and corrosion resistance than traditional carbon steel, but its corrosion resistance is not as good as stainless steel because it has low amounts of alloy elements. Thus, an anti-corrosion method was needed for this low-alloy steel.

Conversion coating techniques such as phosphating can retard corrosion, improve the adhesion of paints on metals, and lengthen the life of the following coatings. These are also an important pretreatment process for metal coatings[12-14]. Substrate surface preparation strongly affects the quality of the conversion coating. The effect of surface roughness on the conversion coating has been widely reported[15,16]. Bogi and Machillan reported that rough surfaces, e.g. heavily abraded or grit-blasted, offer many high surface energy sites and fine irregular crystals. A smooth pickling surface formed large crystals; a smoother polished surface produced to a fine crystalline deposit[12]. The conversion coating is divided into chemical conversion coatings and electrochemical conversion coatings based on the preparation technique[17]. It has been widely reported that nanocrystalline structures can change the characteristics of the passive film on stainless steel samples<sup>[18,19]</sup>. However, the effects of surface nanocrystallization on the chemical and electrochemical conversion coating on non-passivated steel are largely unknown.

In the present work, a nanocrystalline layer was fabricated by high-energy shot peening on the surface of a low-alloy steel 15CrMo. Then, a chemical conversion coating and an electrochemical conversion coating are separately formed on the different samples. By comparing their morphology and corrosion behavior, the effect of surface nanocrystallization of steel substrate on properties of the chemical conversion coating and the electrochemical conversion coating will be systematically investigated. These results are important for the application of surface nanocrystallization techniques to strengthen steel corrosion resistance.

## 2. EXPERIMENTAL DETAILS

### 2.1 Materials

A low-alloy steel (15CrMo) with a chemical composition (wt.%) of 0.13 C, 0.22 Si, 0.56 Mn, 0.005 S, 0.014 P, 0.92 Cr, 0.13 Mo, 0.04 Cu, 0.04 Ni, 0.01 V, 0.03 Al, and the remainder Fe was used as the raw material. The steel was cut into 10 mm × 15 mm × 5 mm samples. The steel surface was processed by abrading with 400-grit SiC paper, polishing using 0.5 μm Al<sub>2</sub>O<sub>3</sub> power, treating in 50 vol.% HCl solution following polishing, and high-energy shot peening, respectively. The high-energy shot peening process was conducted for 20 min at 0.4 MPa using 0.05-mm diameter stainless particles as the peening ball with a peening distance of 4.5 cm.

### 2.2 Specimen processing

The chemical conversion process was conducted at 75 °C for 10 min in a solution prepared by addition of 6 g/L zinc oxide, 2 g/L citric acid, 1 g/L sodium fluoride, 1 g/L nickel nitrate, 1 g/L tartaric acid, 3 g/L sodium chlorate, 4 ml/L formaldehyde, and 18 ml/L phosphoric acid to distilled water.

The electrochemical conversion process was conducted at 25 °C in a solution prepared by addition of 60 g/L zinc nitrate, 60 g/L zinc dihydrogen phosphate, 1 g/L tartaric acid, 5 g/L citric acid, and 2 g/L triethanolamine to distilled water. The electrochemical conversion process was performed in a two-electrode system containing a cathode (low-carbon steel exposed area of 1.5 cm<sup>2</sup>) and an anode (lead plate with 28 cm<sup>2</sup>). A galvanostat applied a constant current density (10 mA·cm<sup>-2</sup>) to the electrochemical phosphating cell for 15 min.

### 2.3 Test methods

The microstructures of the steel base samples were observed by optical microscopy and transmission electron microscopy (TEM, Tecnai G2). The TEM samples were prepared by a twin-jet polishing technique consisting of an electrolyte solution containing 20% perchloric and 80% methanol; the potential and operating temperatures were 40 V and -40 °C, respectively. The surface morphology and elemental distribution characteristics of the steel base samples before and after high-energy peening were analyzed by scanning electron microscope (SEM) and energy disperse spectroscopy (EDS) coupled to SEM.

The surface morphology of all the prepared conversion coatings was observed with SEM. The film composition was analyzed by EDS and X-ray diffraction (XRD) from 10-60° at a scan rate of 4 °/min.

Potentiodynamic polarization tests were performed at 20°C using a Zahner Im6ex electrochemical station in a 3.5 mass% NaCl solution. A conventional three-electrode cell was constructed using the coating sample as the working electrode, a saturated calomel electrode (SCE) as the reference electrode, and a 15 mm × 15 mm platinum foil as the auxiliary electrode. The polarization data were acquired at a sweep rate of 0.3 mV s<sup>-1</sup> from the open circuit potential to an overpassivation potential. The surface morphology data of the film samples after 28 days of immersion corrosion in a 3.5 mass% NaCl solution were observed via macroscopic analysis. Three parallel samples were carried out for all experimental tests.

## 3. RESULTS AND DISCUSSION

### 3.1 Characteristics of nanocrystalline layer

#### 3.1.1 Microstructure characteristics

Figure 1 shows the microstructure of the original unpeened steel and the high-energy shot-peened steel. The microstructure of the original sample consists of ~20 vol.% pearlite (dark phase; Fig. 1a); the remainder is ferrite (bright phase) with an average grain size of about 4 μm; the pearlite lumps are randomly distributed in the matrix. The microstructure of the shot-peened surface is shown in Fig. 1b—the ferrite grain boundaries and grain sizes are difficult to identify by optical microscopy, and the

pearlite lumps are severely deformed, curled, and redistributed. Higher resolution analytical equipment is needed to distinguish the detailed structure of the deformed layer.

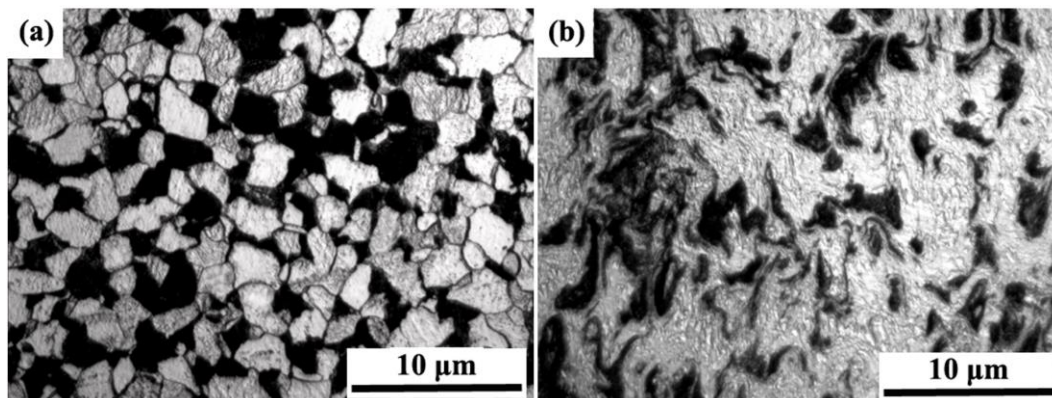


**Figure 1.** Microstructure of 15CrMo steel: (a) original unpeened sample. (b) high-energy shot-peened sample.

Figure 2 shows TEM bright-field micrographs of the top surface layer of the shot-peened sample. After high-energy shot peening, a mass of cell block structures with an average size of 100 nm were observed. Parts of the cell blocks had many high density dislocations. Although sharp grain boundaries were not observed around the cell blocks in Fig. 2a, the corresponding SAED pattern shows diffraction rings indicating that large angle grain boundaries were formed. The TEM results indicate that a nanocrystalline (NC) layer of the steel substrate is fabricated via the high-energy shot peening. This results in a large amount of crystalline defects including dislocations and grain boundaries.

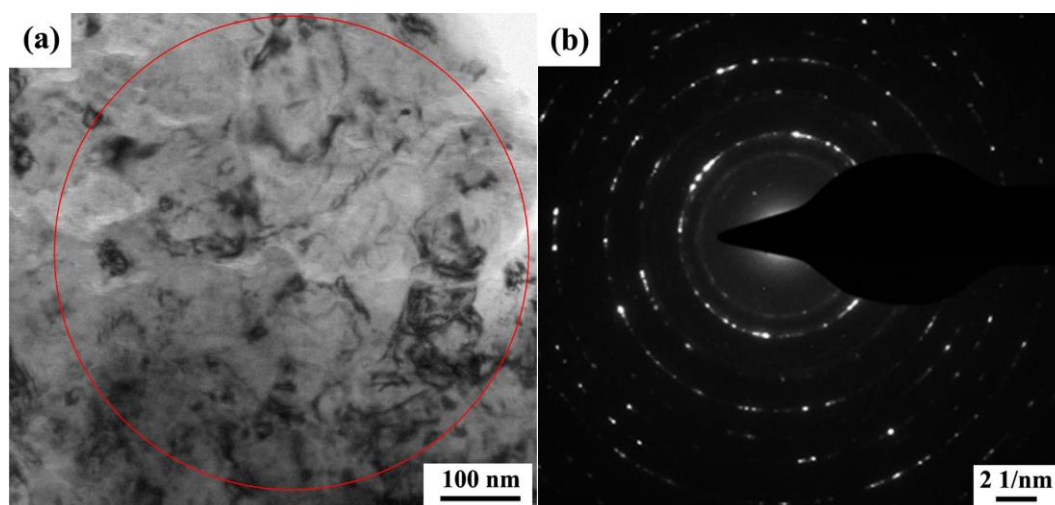


**Figure 2.** TEM images of the top surface layer on the high-energy shot-peened steel: (a) microstructure morphology; (b) the corresponding SAED pattern of (a).

### 3.1.2 Elemental distribution

Figure 3 shows that the Cr and Mo alloys were distributed in the original coarse-grained (CG) and shot-peened nanocrystalline (NC) 15CrMo steel. The high-energy shot peening increased the content of Cr and Mo in the top surface layer of 15CrMo steel (Fig. 3 (same magnification)). The distribution of Cr and Mo elements in the NC layer was more uniform than those in the CG sample. If the Cr and Mo passive alloy elements joined to form a conversion coating, then it could affect the corrosion resistance of the conversion coating. Thus, the surface NC layer can largely improve the surface activity and change the atomic distribution characteristic of the steel. This may have unknown and important effects on the formation process and properties of the surface conversion coating. The effect degree of the NC structure on the conversion coating is related to the type of the conversion coating.

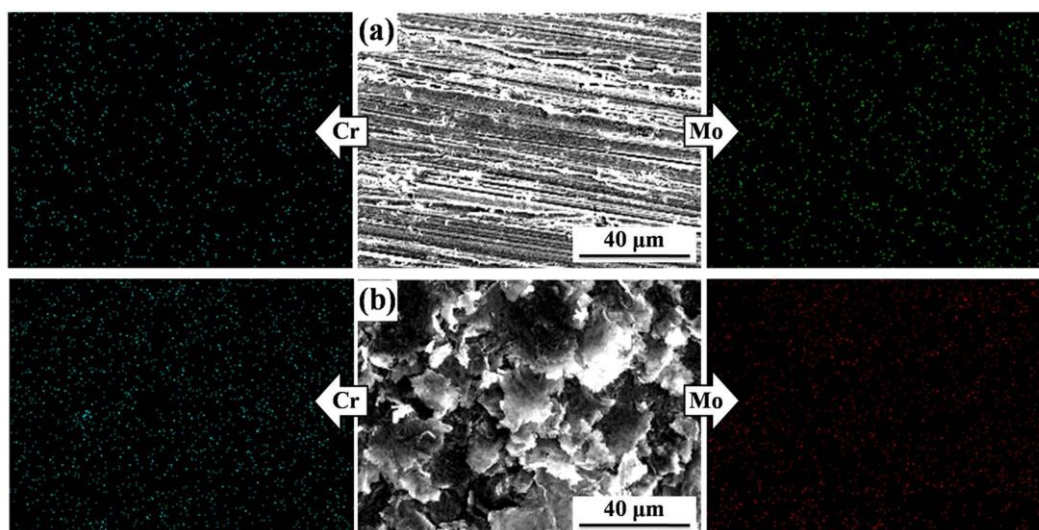


**Figure 3.** Cr and Mo elemental distribution maps of the different steel substrates obtained by EDS: (a) the original unpeened coarse-grained steel sample; (b) the high-energy shot-peened nanocrystalline steel sample.

## 3.2 Properties of chemical conversion coating

### 3.2.1 Morphology characteristics

Fig. 4 shows the SEM morphologies of the chemical conversion coatings on the unpeened CG and peened NC steel. The morphology of the chemical conversion coating obviously changed due to the high-energy shot peening processing of the steel base (Fig. 4). The chemical conversion coating on the original coarse-grained steel (Fig. 4(a)) has blocky crystalline particles with an average size of 10 μm. The surface of the film on the original steel base was uneven and has some holes between crystalline particles (directed by the arrow A in Fig. 4(a)). The crystallized particle features are not seen in the chemical conversion coating on the surface of the nanocrystalline steel. The film shows irregular flocculents composed of fine particles (Fig. 4(b)).

The chemical conversion coating changes the grain refinement of the steel base. The crystalline defects include grain boundaries and dislocations. This is increased by the shot peening process that increases the surface activity of the steel and the number of nucleation sites in the conversion coating. The formation process of the chemical conversion coating on the coarse-grained steel was as following: after initial nucleation, the particles grew and contacted each other. The particles formed after chemical conversion coating on the nanocrystalline steel do not have sufficient time to grow after initial nucleation. There are very small and aggregated particles.

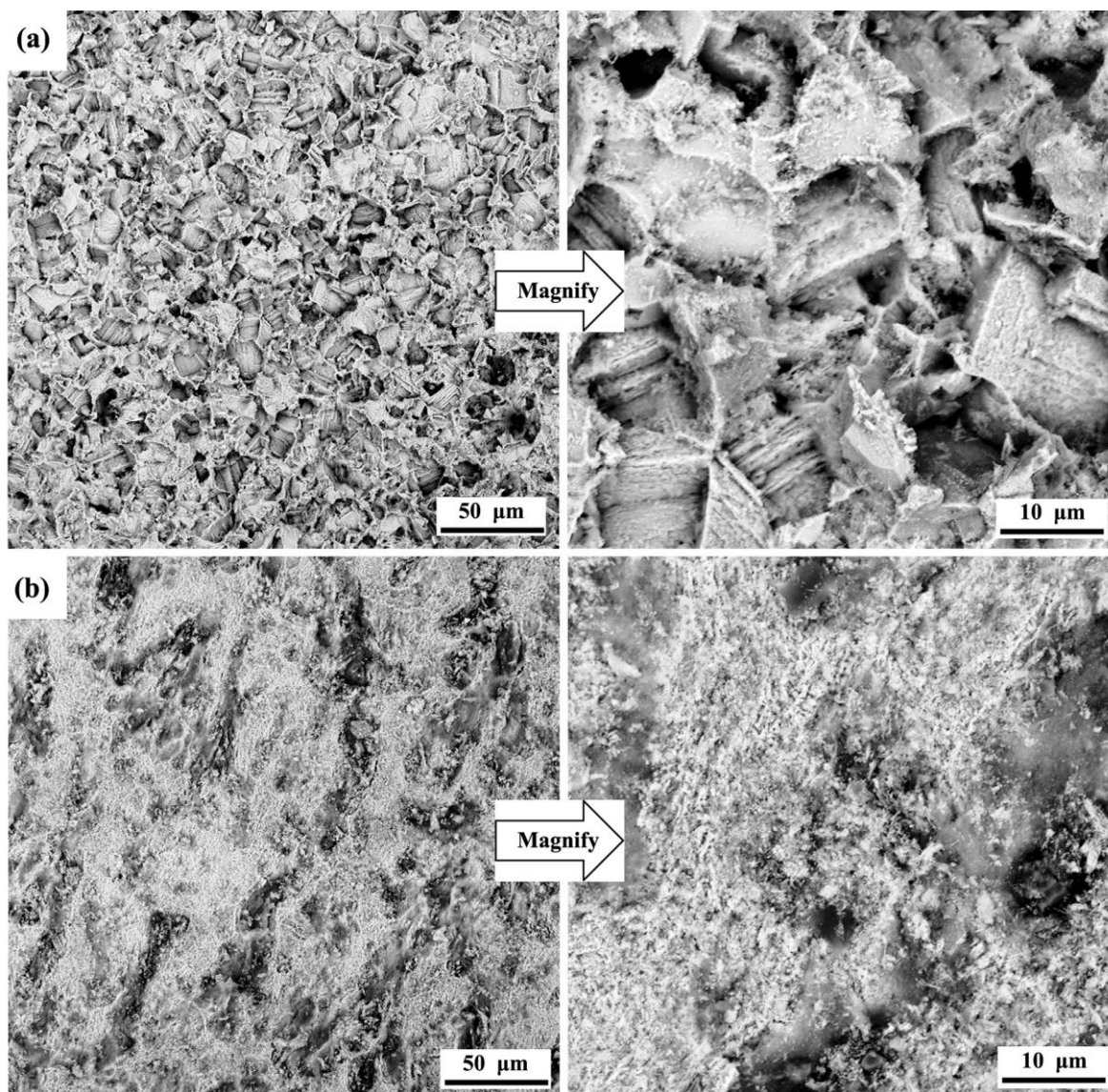


**Figure 4.** SEM images of the chemical conversion coating on the different steel substrates: (a) the original unpeened coarse-grained steel substrate; (b) the high-energy shot-peened nanocrystalline steel substrate.

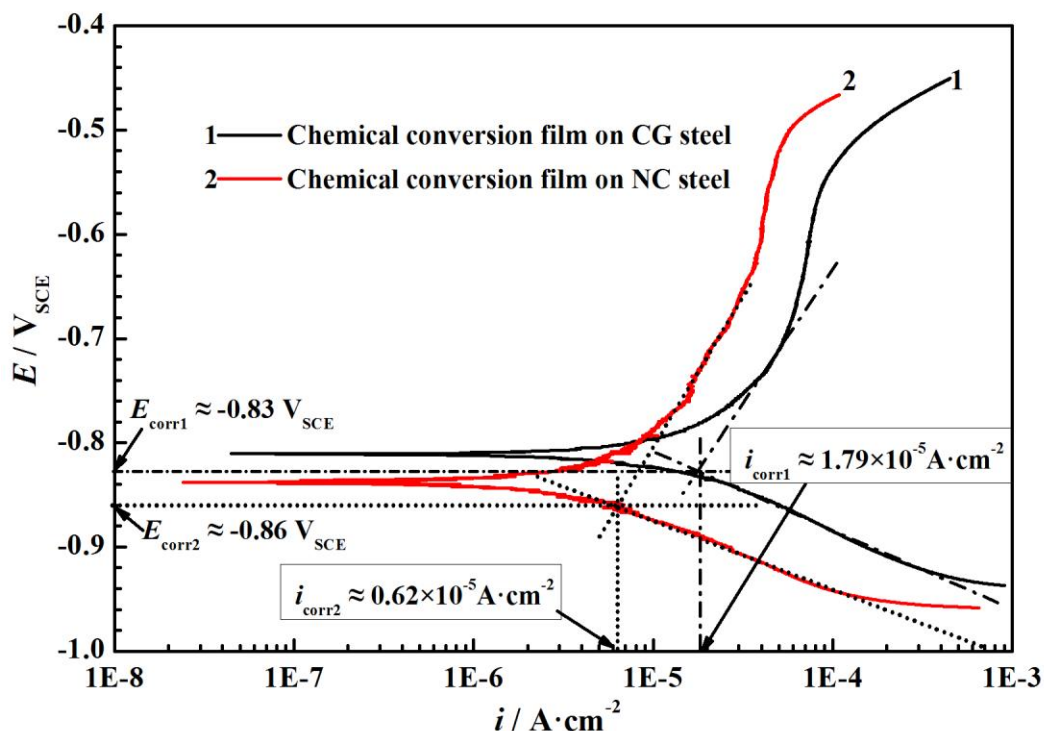
Table 1 shows the average content of the main elements in the chemical conversion coating on the surface of the original unpeened sample and the shot-peened sample.

**Table 1.** Element content (mass%) of the chemical conversion coating on the CG and NC steel substrates.

Element	Chemical conversion coating on CG steel base	Chemical conversion coating on NC steel base
Fe	80.40	75.15
O	16.25	15.40
P	1.00	2.40
Cr	1.05	2.10
Mo	1.80	3.10
Zn	0	1.45
Al	0	0.90

The elemental composition and content of the film on the unpeened sample are obviously different from the shot-peened sample (Table 1). Nanocrystallization of the steel substrate resulted in a film on the steel. The ferrum content decreased from 80.4% to 75.15%, the oxygen decreased slightly, the phosphorus, chromium, and molybdenum obviously increased, and traces of zinc and aluminum appeared. More alloy elements from the steel substrate participated in the conversion coating and formation process. This suggests that the atomic reactivity was enhanced, and the reaction channels were increased via nanocrystallization of the steel substrate. The alloy elements with self-passivation ability include Cr, Mo, and Al; they can improve corrosion resistance.

3.2.2 Corrosion behavior



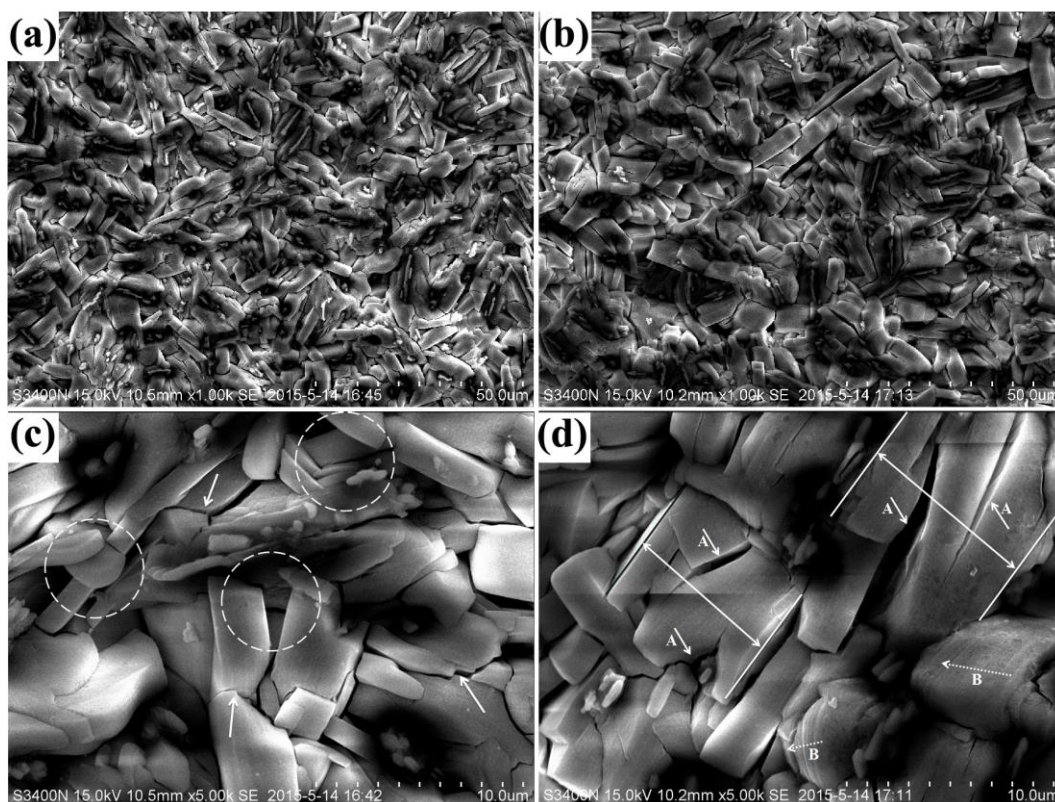
**Figure 5.** Polarization curves of the chemical conversion coating on the CG and NC steel substrates in the 3.5 mass% NaCl solutions at 20°C.

Fig. 5 shows the polarization curves of the chemical conversion coating on the surface of the original CG sample and the NC sample; these are similarly shaped but have a different position.

The polarization curve of the film is shifted to the bottom left after the steel nanocrystallization process. There is only a small movement, which means that the change in free corrosion potential ( $E_{\text{corr}}$ ) is minor. The left moving of the polarization curve indicates a decrease in the free corrosion current density ( $i_{\text{corr}}$ ) of the film on the NC steel. Figure 5 shows calculated results for the  $i_{\text{corr}}$  values of the chemical conversion coating on the surface of the original unpeened sample and the shot-peened sample. The  $i_{\text{corr}}$  value of the chemical conversion coating decreased from  $1.79 \times 10^{-5} \text{ A}\cdot\text{cm}^{-2}$  to  $0.62 \times 10^{-5} \text{ A}\cdot\text{cm}^{-2}$  by nanocrystallization of the steel substrate. The decrease in  $i_{\text{corr}}$  indicates the corrosion resistance of the chemical conversion coating is improved by nanocrystallization process of the steel substrate. The chemical conversion coating on the NC steel has higher corrosion resistance due largely to the self-passivation elements joined at the film and the dense structure of the film.

### 3.3 Properties of electrochemical conversion coating

#### 3.3.1 Morphology and component



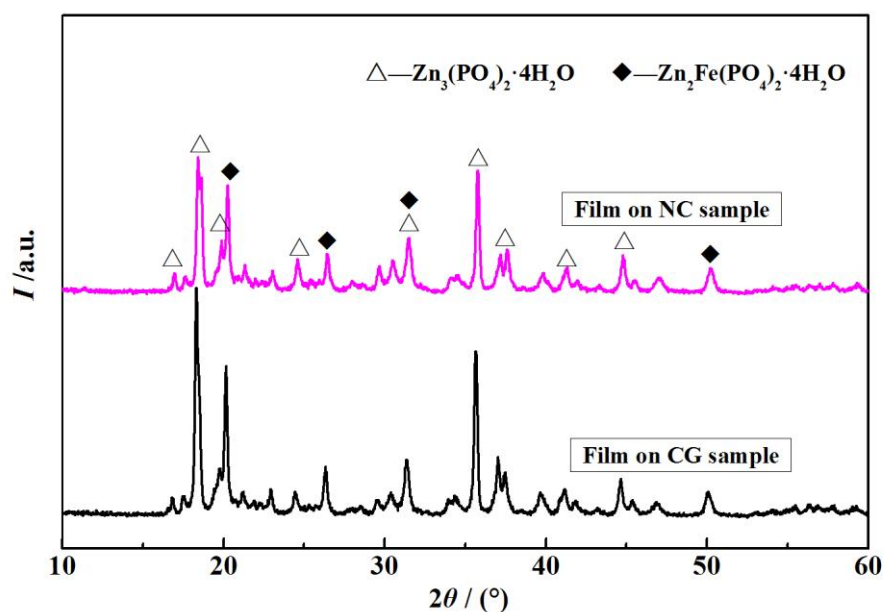
**Figure 6.** SEM images of the electrochemical conversion coating on the different steel substrates: (a) CG sample; (b) NC sample; (c) magnification of (a); and (d) magnification of (b).

Figure 6 shows the SEM morphologies of the electrochemical conversion coatings applied on the CG and the NC steel substrates. The films on the CG and the NC substrates have similar character—uniform and containing many finer blocky crystalline particles (Figs. 6a and 6b). The

microscopic details of the electrochemical conversion coatings applied to the CG and the NC steel substrates are different and are shown in Figs. 6c and 6d. Some micro-cracks are observed on the crystalline particles (marked by the arrows Fig. 6c), and the two sides of the cracks can occlude well, which indicates that the crystalline particle will crack when it is grown to a certain size.

The dotted circles in Fig. 6c show that the top crystalline particle layer overlays the lower crystalline layer. We suspect that the formation process of the electrochemical conversion coatings applied to the CG is layer-by-layer growth.

As shown in Fig. 6d, the ladder-shaped parallel lines in the same direction are observed in the some crystalline particles (marked by the arrows B). The micro-cracks are observed on the crystalline particles (marked by the arrows A), and the two sides of the cracks can occlude well. This indicates that the crystalline particle will crack when grown to a certain size. The crystalline particles of the film on the NC substrate have a block-like shape, while those on the CG substrate are long bars. The layer-by-layer growth phenomenon was not appeared in the film forming process on the NC substrate. Figure 7 shows the XRD patterns of the electrochemical conversion coatings on the coarse-grained and nanocrystalline steel substrates.



**Figure 7.** XRD patterns of the electrochemical conversion coating on the CG and NC steel substrates.

Fig. 7 shows that the peak positions do not change, but the peak strength is decreased. This indicates that the crystallinity or content of the composition phases in the films are different. The electrochemical conversion coatings on the coarse-grained and nanocrystalline steel substrates are the same:  $\text{Zn}_3(\text{PO}_4)_2 \cdot 4\text{H}_2\text{O}$  and  $\text{Zn}_2\text{Fe}(\text{PO}_4)_2 \cdot 4\text{H}_2\text{O}$ . The peak strength of the film on its surface decreases after surface nanocrystallization of steel substrate.

## 3.3.2 Corrosion behavior

Figure 8 shows the polarization curves of the electrochemical conversion coatings on the steel substrates with and without surface nanocrystallization. They have a similar shape but on different positions. The electrochemical parameters including free corrosion potential ( $E_{\text{corr}}$ ) and free corrosion current density ( $i_{\text{corr}}$ ) are prepared by simulating the polarization curves (Fig. 8).

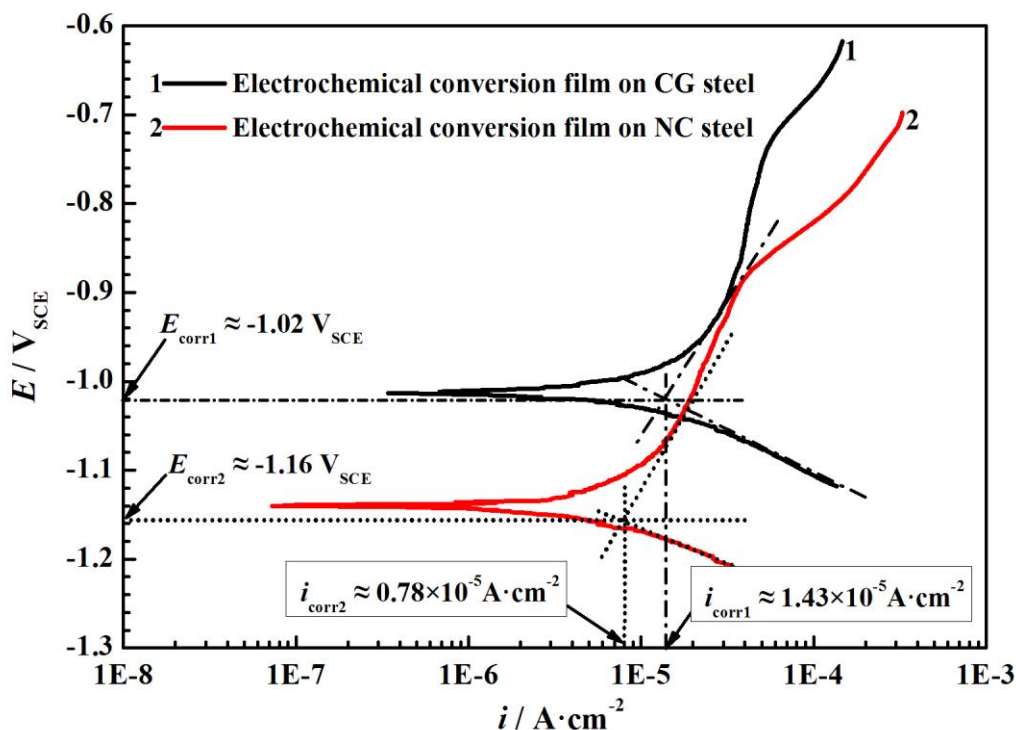


**Figure 8.** Polarization curves of the electrochemical conversion coating on the CG and NC steel substrates in the 3.5 mass% NaCl solutions at 20°C.

Versus the polarization curve of the film on the coarse-grained steel, the polarization curve of the film on the nanocrystalline steel moved left suggesting that its corrosion rate decreased (Fig. 8). The  $i_{\text{corr}}$  value of the film on the coarse-grained steel is  $1.43 \times 10^{-5} A \cdot cm^{-2}$ , while  $i_{\text{corr}}$  value of the film on the nanocrystalline steel is  $0.78 \times 10^{-5} A \cdot cm^{-2}$ . This is only about one half of the film on the coarse-grained steel. Thus, the film on the nanocrystalline sample has higher corrosion resistance than that of on the coarse-grained steel.

Figure 9 shows the macro morphologies of the electrochemical conversion coating on the steel substrates with and without surface nanocrystallization after 28 days of immersion corrosion in 3.5 mass% NaCl. The film on the coarse-grained steel seriously corrodes, and a large part detaches (Fig. 9a). There are many corrosion pits on the non-peeling part of the film. On the surface of the coarse-grained steel, the electrochemical conversion coating has poor adhesion. This shows obvious brittle delamination. The film on the NC sample has some pitting corrosion, but the film adhered firmly on the substrate without showing any peeling phenomena (Fig. 9b).

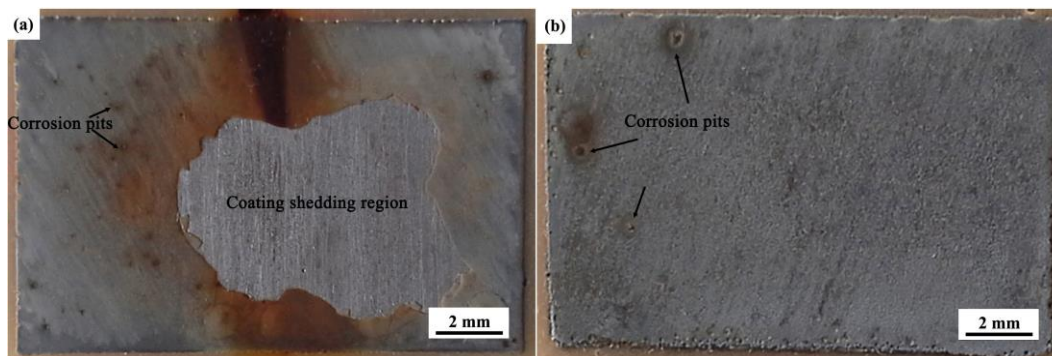


**Figure 9.** Corrosion morphologies of the film after 28 days of immersion in 3.5 mass% NaCl on the different treated steel substrates: (a) the original unpeened coarse-grained steel substrate; (b) the high-energy shot-peened nanocrystalline steel substrate.

Both the polarization and immersion tests results indicate that the surface nanocrystallization treatment of the steel forms an electrochemical conversion coating with good corrosion resistance.

### 3.4 Discussion

The surface nanocrystallization of the steel substrate has different effects on the characteristics of the chemical conversion coating and electrochemical conversion coating. After the surface nanocrystallization of the 15CrMo steel substrate, the structure of chemical conversion coating on its surface was transformed from the regular crystallized particles, and more alloy elements participated in the film. The film formation features of the electrochemical conversion coating changed less dramatically. The different effects are due to the different formation mechanisms between the chemical conversion coating and electrochemical conversion coating.

The formation mechanism of the conventional chemical conversion coating has been revealed[12]. The formation process of the chemical conversion coating on the coarse-grained steel was as follows—after initial nucleation, the particles grew and contacted each other. For the formation mechanism of the chemical conversion coating, the alloy elements of the steel substrate partially joined in the film forming reaction and transformed into the metal phosphate and metal oxide[20]. Thus, the Cr and Mo elements enriched to the surface of the steel after nanocrystallization, which have more chance to be transformed into the conversion coating. The pearlite in the steel also affected the structure of the conversion coating. The increase in pearlite resulted in a coarsening of the crystals in the conversion coating[21]. The refinement of the pearlite in the steel after shot peening increased the continuity of the conversion coating because the crystal nuclei develop only somewhat on the islands of pearlite. The crystalline defects including grain boundaries and dislocations were increased in the steel after nanocrystallization; the initial metal attack occurred preferentially[20]. The increased crystalline defects improved the number of the crystal nuclei of the conversion coating. The particles of the chemical conversion coating on the NC steel do not have enough time to grow after the initial nucleation. This shows the amorphous character resulting from aggregation of the fine particles. Some

authors[22-24] showed that the grain refinement of the steel after heat treatment or machining improved the deposition rate of the conversion film.

The alloy elements of the steel substrate did not form the electrochemical conversion coating in contrast to the formation mechanism of the conversion coating. The steel substrate was the cathode during the formation of the electrochemical conversion coating. This resulted in a large number of electrons with an external power. The  $H^+$  ions near the steel surface captured the electrons and caused hydrogen evolution. Thus, the pH value increased, and this accelerated the deposition of  $PO_4^{3-}$  at the steel surface. The phosphates were then supersaturated and deposited to form a coating that covered the steel surface. The formation mechanism of the conversion coating was not markedly affected by the properties of the steel substrate. Thus, the morphology and phases of the electrochemical conversion coating on the surface of the CG steel and the NC steel were almost identical. The morphology of the electrochemical conversion coating were mostly affected by bath composition, current density, processing time, pH value, and temperature[25].

Interestingly, the deposition position and number of the crystal nuclei was affected by the surface properties of the steel substrate[4]. The NC steel with large numbers of crystalline defects has a higher surface energy that occurred preferentially during nucleation. Due to the large number of nucleation positions on the NC surface, the electrochemical conversion coating adhered strongly to the NC steel surface. This is rarely reported by other authors. Thus, the electrochemical conversion coating strongly adhered to the NC steel and showed a higher resistance to salt water than the coating on the CG sample.

#### 4. CONCLUSIONS

Low-alloy steel 15CrMo with a surface nanocrystalline layer was fabricated via high-energy shot peening. The morphology and corrosion behavior of a chemical conversion coating as well as an electrochemical conversion coating were evaluated.

(1) After surface nanocrystallization of 15CrMo steel, the main changes of the chemical conversion coating on its surface was the amorphization of the regular crystallized particles and the participation of more alloy elements in the film; the formation of the electrochemical conversion coating did not markedly change.

(2) The chemical conversion coating on the NC steel had a higher corrosion resistance than the CG steel due to the self-passivation elements joining the film and the dense structure of the film.

(3) The electrochemical conversion coating on the NC steel had a higher corrosion resistance than the CG steel due to its stronger adhesion to the substrate.

#### ACKNOWLEDGEMENTS

This work was financially supported by the National Natural Science Foundation of China (51709049), and the Science and Technology Plan of Guangdong Province China (2016A010103034).

#### References

1. K.S. Siow, A.A.O. Tay and P. Oruganti, *Mater. Sci. Tech.*, 20(2004) 285.

2. I. Roy, H.W. Yang, L. Dinh, I. Lund, J.C. Earthman and F.A. Mohamed, *Scripta Mater.*, 59(2008) 305.
3. G. Liu, S.C. Wang, X.F. Lou, J. Lu and K. Lu, *Scripta Mater.*, 44(2001) 1791.
4. H. Li, Y. Liu, M. Li and H. Liu, *Appl. Surf. Sci.*, 357(2015) 197.
5. Y. Liu and M. Li, *Mat. Sci. Eng A-Struct.*, 669(2016) 7.
6. D. Li, H.N. Chen and H. Xu, *Appl. Surf. Sci.*, 255(2009) 3811.
7. H.W. Huang, Z.B. Wang, J. Lu and K. Lu, *Acta Mater.*, 87(2015) 150.
8. Z.M. Blednova and P.O. Rusinov, *Applied Mechanics & Materials.*, 592-594(2014) 1325.
9. K.D. Ralston and N. Birbilis, *Corrosion*, 66(2010) 0750051.
10. K.D. Ralston, N. Birbilis and C.H.J. Davies, *Scripta mater.*, 63(2010) 1201.
11. L. Liu, Y. Li and F.H. Wang, *J. Mater. Sci. Technol.*, 26(2010) 1.
12. J. Bogi and R. Macmillan, *J. Mater. Sci.*, 12(1977) 2235.
13. S. Rebeyrat, J.L. Grosseau-Poussard, J.F. Silvain, B. Panicaud and J.F. Dinhut, *Appl. Surf. Sci.*, 199(2002) 1.
14. B. Ramezanzadeh, H. Vakili and R. Amini, *Appl. Surf. Sci.*, 327(2015) 174.
15. S. C. Lee, W. Y. Ho and F. D. Lai, *Materials Chemistry & Physics*, 43(1996)266.
16. M. Wolpers and J. Angeli, *Appl. Surf. Sci.*, 179(2001) 281.
17. S. Jegannathan, T. K. Arumugam, T. S. N. Sankara Narayanan and K. Ravichandran., *Prog. Org. Coat.*, 65(2009) 229.
18. Y. Gui, Z. J. Zheng and Y. Gao, *Thin Solid Films*, 599(2016) 64.
19. Z. J. Zheng, Y. Gao, Y. Gui and M. Zhu, *J. Solid State Electr.*, 18(2014) 2201.
20. T. S. N. Sankara Narayanan, *Rev. Adv. Mater. Sci.*, 9(2005)130.
21. K. A. Akanni, C. P. S. Johal and D. R. Gabe, *Transactions of the Imf*, 62(1984)64.
22. T. Hada, S. Naito, K. Ando and M. Yoneno, *J. Surf. Finish. Soc. Japan*, 41 (1990) 844.
23. H. Schuemichen, In: Proceedings of the Interfinish, 84 (Tel Aviv, Israel, 1984) p. 411.
24. P.E. Augusston, I. Olefjord and Y. Olefjord, *Mater. Corros.*, 34 (1983) 563.
25. S. Jegannathan, T.S.N.S. Narayanan, K. Ravichandran, S. Rajeswari, *Surf. Coat. Tech.*, 200 (2006) 6014.